

# Hopping and microscopic dynamics of ultrasoft particles in cluster crystals

Daniele Coslovich,<sup>\*</sup> Lukas Strauss,<sup>†</sup> and Gerhard Kahl

*Institut für Theoretische Physik and Center for Computational Materials Science (CMS),  
Technische Universität Wien, Wiedner Hauptstraße 8-10, A-1040 Wien, Austria*

(Dated: November 6, 2018)

We have investigated the slow dynamics of ultrasoft particles in crystalline cluster phases, where point particles interact through the generalized exponential potential  $u(r) = \epsilon \exp[-(r/\sigma)^n]$ , focusing on the cluster fcc phase of this model with  $n = 4$ . In an effort to elucidate how the mechanisms of mass transport depend on the microscopic dynamics and in order to mimic a realistic scenario in a related experiment we have performed molecular dynamics, Brownian dynamics, and Monte Carlo simulations. In molecular dynamics simulations the diffusion of particles proceeds through long-range jumps, guided by strong correlations in the momentum direction. In Monte Carlo and Brownian dynamics simulations jump events are short-ranged, reflecting the purely configurational nature of the dynamics. In contrast to what was found in models of glass-forming liquids, the effect of Newtonian and stochastic microscopic dynamics on the long-time relaxation cannot be accounted for by a temperature-independent rescaling of the time units. From the obvious qualitative discrepancies in the short time behavior between the three simulation methods and the non-trivial difference in jump length distributions, long time relaxation, and dynamic heterogeneity, we learn that a more complex modeling of the dynamics in realistic systems of ultrasoft colloids is required.

PACS numbers: 61.20.Ja, 64.70.pv, 82.70.Dd

## I. INTRODUCTION

Although the formation of stable clusters of particles that interact via entirely repulsive, ultrasoft potentials might seem counterintuitive at first sight, it is by now well established that cluster phases of such systems *do* exist [1–6]. This phenomenon is potentially relevant for a wide class of ultrasoft colloidal systems, such as dendrimers and microgels, in which the centers of mass of the colloidal particles can overlap with a finite energy cost. Theoretical considerations [7] in combination with computer simulations [8] for models of ultrasoft colloidal particles have given evidence for the existence of these clusters and have, in addition, provided a deeper understanding of this phenomenon. Stable clusters form either in disordered, liquid-like phases or occur as ordered cluster crystals where the particle aggregates populate the lattice sites of regular fcc or bcc lattices. Most of the investigations have been dedicated up to now to study the static properties of the cluster phases, of which we mention the two most remarkable ones: (i) freezing and melting lines depend in a linear way on the density and (ii) the lattice constant of cluster crystals is invariant under compression, inducing thereby a linear growth of the cluster size with density.

In contrast, little effort has been dedicated, so far, to obtain a deeper insight into the dynamics that governs these cluster forming systems. To the best of our knowledge, only two contributions that deal with the diffusion and the relaxation dynamics in cluster crystals have been published [9, 10]. From these investigations, based on

molecular dynamics (MD) simulations, it became clear that the dynamics in cluster crystals shows features at least as intriguing as their static counterparts. For instance, these investigations revealed that particles move constantly between neighboring clusters, while maintaining the original lattice structure of the cluster crystal and the average cluster population on the lattice sites. Further, a closer analysis of the dynamic correlation functions provided evidence for a decoupling between self and collective time-dependent correlations [9].

The present contribution is dedicated to investigate the dynamical properties of ultrasoft particles in a crystalline cluster phase in detail and from a more general point of view. In particular, we intend to study how mass transport is realized in different simulation schemes, which mimic different scenarios in related realistic systems: (i) in MD simulations, where the influence of the microscopic solvent is neglected and the mesoscopic (colloidal) particles move according to Newton’s law; (ii) in Monte Carlo (MC) simulations, where the random collisions of the colloids with the solvent particles are mimicked through the stochastic nature of the algorithm; (iii) in Brownian dynamics (BD) simulations, where the influence of the solvent is taken into account via the friction term and the stochastic forces acting on the particles.

The model system that we choose to study cluster phases is the generalized exponential model of index  $n$  (GEM- $n$ ) [3], in which particles interact via the potential

$$\Phi(r) = \epsilon \exp[-(r/\sigma)^n]. \quad (1)$$

In the literature, this model has been used to describe the effective interactions between linear polymer chains ( $n = 2$ ) [11] and dendrimers ( $n \approx 3$ ) [12] in the dilute regime. For  $n > 2$ , we expect this model to capture the

---

<sup>\*</sup>Corresponding author: daniele.coslovich@univ-montp2.fr

<sup>†</sup>D. Coslovich and L. Strauss contributed equally to this work.

general features of purely repulsive, cluster-forming systems [5]. In contrast to Ref. [9], where  $n = 8$  was considered, we have based our investigations on the GEM-4 system, for which highly accurate data for the phase diagram are available [3, 8]. In a first step, we have focused on the microscopic dynamics and on the jump events, comparing MD and MC dynamics. We have found distinct differences between these two types of dynamics imposed by the simulation technique: in MC simulations, hopping takes place only over short distances (i.e., essentially from one cluster to a neighboring one); in contrast, in MD simulations particles can migrate over large distances through the crystal. Furthermore, our investigations on the diffusion constant and on the dynamic correlation functions have shown that properties calculated from MD and MC *cannot* be superposed by a simple, temperature-independent rescaling of time. This finding is in striking contrast to what is known from normal [13, 14] or glass-forming [15–17] liquids. Finally, we have found that BD simulations give rise to dynamical properties very similar to those observed in MC simulations, supporting the view that MC dynamics effectively (although approximately) incorporates solvent effects [18–20]. Our results indicate that a complex dynamical scenario may arise as a competition of activated processes and momentum correlations, and suggest that the solvent properties may change qualitatively the nature of the slow dynamics in cluster-forming colloidal systems.

The paper is organized as follows: in Section II we introduce the model and present our simulation methods; in Section III we present our results for the dynamical properties of a GEM-4 cluster crystal and finally in Section IV we give our conclusions. In the Appendix we present our algorithm for cluster identification.

## II. MODEL AND METHODS

Our model is composed of  $N$  classical particles of mass  $m$  enclosed in a cubic box with periodic boundary conditions. Particles interact through the generalized exponential potential, Eq. (1), with  $n = 4$ . The potential is truncated and shifted at  $r_c = 2.2\sigma$ . In the following, we will use the parameters  $\sigma$  and  $\epsilon$  in Eq. (1) as units of distance and energy, respectively. The units of time are chosen differently according to the simulation method (see below). For each studied density in the fcc cluster phase (see Fig. 1), the *equilibrium* value of  $N$  was determined using the algorithm developed in Ref. [8], yielding  $N = 3367$  for  $\rho = 6.4$ . During this procedure, we used an fcc cluster crystal comprising four unit cells per side. We have checked that size effects do not play a relevant role by performing simulations on smaller systems, i.e., using three unit cells per side.

The dynamical properties of the model were investigated using MD, MC, and BD simulations. MD simulations were performed in the  $NVE$  ensemble with fixed center of mass using the velocity-Verlet algorithm [21].

Equilibration at various temperatures was achieved by reselecting the velocities of particles at regular time intervals according to the appropriate Maxwellian distribution. MC simulations were performed in the  $NVT$  ensemble using the standard Metropolis algorithm. Attempted moves involved only single particle displacements, randomly generated over a cube of side 0.6. The acceptance ratio ranged from 64 % (at high  $T$ ) to 42 % (at low  $T$ ). At any fixed  $T$ , the acceptance ratio decreases monotonically with the length of the maximum attempted displacement. Thus, in contrast to what found for a model glass-forming liquid [15], it is not possible to define an “optimal” value of the maximum attempted displacement. The value chosen in this work is a reasonable compromise between efficiency of the simulation and physical realism. BD simulations were performed by integrating a set of coupled, inertia-free Langevin equations using a simple Euler algorithm [21]. We used a friction parameter  $\xi = 10^{-3}$  (in reduced units) and a temperature-dependent time step  $\delta t_{\text{BD}}$ .  $\xi$  was chosen sufficiently small that the dynamical properties at high  $T$  no longer depend on  $\xi$ . To avoid artifacts in the dynamic correlation functions measured during MC and BD simulations, the motion of the center of mass of the system was subtracted out from the particle displacements. In the following, we will use  $\sqrt{m\sigma^2/\epsilon}$  as the unit of time for MD simulations. In these units, the time step  $\delta t_{\text{MD}}$  for the integration of the equations of motion was 0.03. In the case of MC simulations, time will be measured in units of MC sweeps, where one MC sweep corresponds to  $N$  attempted displacement moves. In BD simulations, the time unit will be  $\sigma^2/D_0$ , where  $D_0 = 1/\xi$  is the diffusion coefficient at infinite dilution and unit temperature.  $\delta t_{\text{BD}}$  was adjusted at each state point so that the dynamical properties did not depend on it anymore upon further reduction, and ranged from  $5 \cdot 10^{-6}$  (at low  $T$ ) to  $10^{-8}$  (at high  $T$ ). Procedures to match the time scales of the different simulations will be discussed in Sec. III.

## III. RESULTS

In this section we characterize the dynamical properties of GEM-4 particles in the fcc cluster crystal phase, paying particular attention to jump diffusion processes and to the effects of the different types of microscopic dynamics introduced in Sec. II. We will focus on the behavior of the system as a function of temperature along the isochore  $\rho = 6.4$  (see Fig. 1). If not stated otherwise, in the following we will always refer to this particular density. The investigated temperature range comprises both the stable fcc cluster phase ( $T \lesssim 0.80$ ) and the super-heated regime. In the latter, the underlying fcc crystal structure remained (meta)stable throughout the simulation. We also performed simulations for selected state points at different densities ( $\rho = 4.3$  and  $8.7$ , see Fig. 1) and checked that the expected scaling of dynamic quantities as a function of  $\rho/T$  holds [9]. In the following

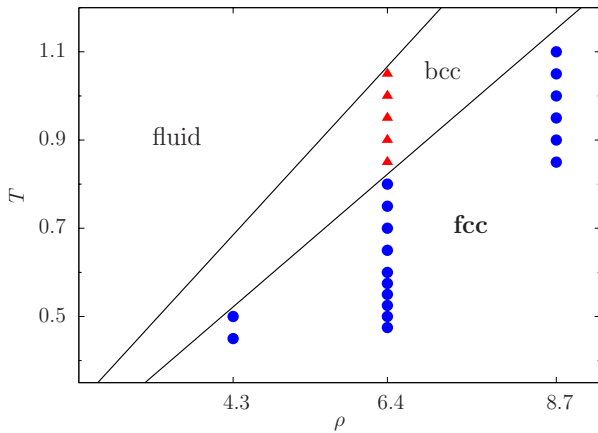


FIG. 1: State points studied in this work in the temperature-density phase diagram. Triangles indicate state points for which the fcc cluster crystal was metastable. The lines between cluster fcc, cluster bcc, and fluid phases of the GEM-4 system have been redrawn from Ref. [3].

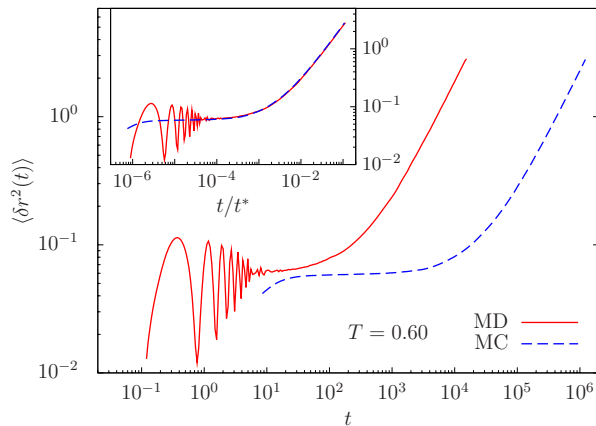


FIG. 2: Main panel: mean square displacement  $\langle \delta r^2(t) \rangle$  as a function of  $t$  at  $\rho = 6.4$  and  $T = 0.60$  from MD (solid line) and MC (dashed line) simulations. Inset: same as main panel but as a function of the rescaled time  $t/t^*$  (see text for definition).

we will therefore use  $\rho/T$  as the natural control parameter of the system. In Sec. III A and III B we will focus our attention on the comparison between MD and MC simulations. In Sec. III C we will discuss the results of BD simulations.

### A. Microscopic dynamics and jump events

We start our discussion with the analysis of the mean square displacement  $\langle \delta r^2(t) \rangle = \langle |\mathbf{r}(t) - \mathbf{r}(0)|^2 \rangle$ . This allows us to review some general features of the dynamics discussed previously for GEM-8 particles [9] and to perform a first comparison of MD and MC simulations. In the main panel of Fig. 2 we show the mean square

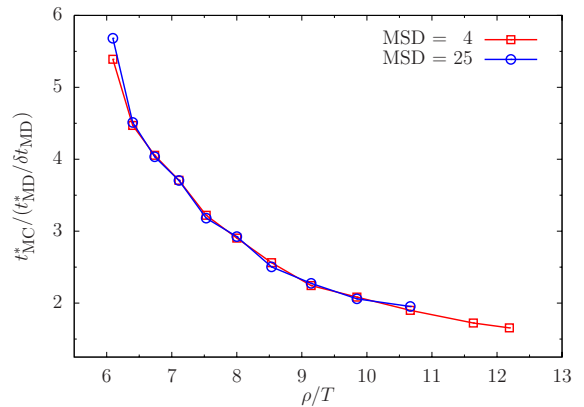


FIG. 3: Time scaling factor  $t_{MC}^*/(t_{MD}^*/\delta t_{MD})$  as a function of  $\rho/T$ .  $\delta t_{MD}$  is the time step used in MD simulations.  $t_{MC}^*$  and  $t_{MD}^*$  are defined as the times at which the mean square displacement equals a fixed target value in MC and MD simulations, respectively. The target values considered are 4 (squares) or 25 (circles).

displacement for a representative state point well within the stable fcc phase ( $\rho = 6.4$ ,  $T = 0.60$ ). After the ballistic time range (not shown here), the MD dataset shows distinct oscillations due to single-particle vibrational modes [5, 9, 22], which disappear for  $t \gtrsim 10$ . At long times, normal diffusion is recovered, i.e.,  $\langle \delta r^2(t) \rangle \sim 6Dt$ . Due to the arbitrary choice of the “time unit” in the case of MC simulations, the respective curve is shifted. It is possible, however, to rescale the time variable,  $t/t^*$ , so that the long time behavior of  $\langle \delta r^2(t/t^*) \rangle$  coincides for both types of dynamics. The state-dependent scaling times  $t^*$  are defined, for both dynamics, by the condition  $\langle \delta r^2(t^*) \rangle = 25$ . The precise choice of the “target” mean square displacement is irrelevant as long as this value is within the diffusive regime (see also Fig. 3). The original and the rescaled datasets are shown in the main panel and inset of Fig. 2, respectively. Adopting the rescaled time representation, the mean square displacements obtained from MD and MC dynamics nicely collapse onto a unique curve at long times ( $t/t^* \gtrsim 10^{-4}$ ). Clear discrepancies are found at short times, due to the expected phonon suppression in MC dynamics [15]. Similar rescaling approaches were used in previous works on Lennard-Jones liquids [13, 15]. However, in contrast to what was found in those studies, the ratio of the MD and MC scaling times displays a systematic temperature dependence. This is demonstrated in Fig. 3, where we show the time scaling factor  $t_{MC}^*/(t_{MD}^*/\delta t_{MD})$  for two values of the target mean square displacement. The ratio  $t_{MC}^*/(t_{MD}^*/\delta t_{MD})$  decreases monotonically with  $1/T$  within the explored temperature range. Therefore, it is not possible to set, once and for all, the time conversion factor between the different types of dynamics.

To understand the discrepancy between the thermal behaviors of the system in MD and MC simulations, we analyze in more detail both types of dynamics and iden-

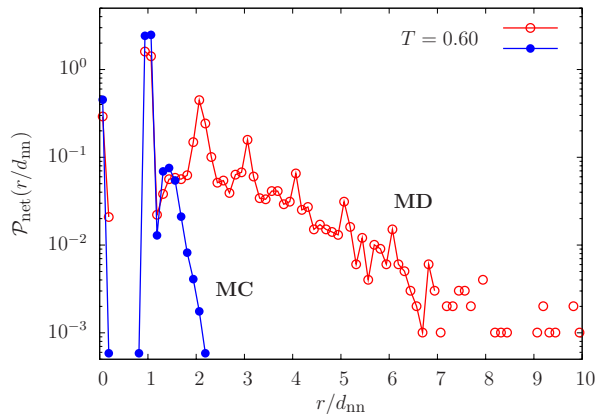


FIG. 4: Distribution of net jump length  $\mathcal{P}_{\text{net}}$  as a function of  $r/d_{\text{nn}}$  at  $\rho = 6.4$  and  $T = 0.60$  for MD (empty circles) and MC (filled circles) simulations.

tify the elementary hopping processes leading to particle diffusion. To this end, we monitor individual particle trajectories and identify jump events by means of the cluster analysis outlined in the Appendix. Our definition of jump events is as follows. At any instant of time  $t$ , we map the position  $\mathbf{r}(t)$  of a tagged particle to the center of mass (CM) of its respective, initial cluster, located at  $\mathbf{R}_{\text{initial}}^{\text{cm}} = \mathbf{R}^{\text{cm}}(t)$ . In MD simulations, a particle is considered “equilibrated” in its respective cluster if the residence time exceeds a characteristic time,  $t_{\text{eq}}^*$ , of the order of a few vibrational periods (cf. Fig. 2). In our calculations at  $\rho = 6.4$ , we chose  $t_{\text{eq}}^* = 3.6$ , independent of temperature. We checked that reasonable variations of  $t_{\text{eq}}^*$  around the selected value by some 10% or 20%, or introduction of a  $T$ -dependent  $t_{\text{eq}}^*$  do not modify qualitatively our analysis. In MC simulations, the equilibration time is given by  $t_{\text{eq}}^*(t_{\text{MC}}^*/t_{\text{MD}}^*)$ , where  $t_{\text{MC}}^*$  and  $t_{\text{MD}}^*$  are the scaling times introduced above. A jump event starts when the tagged particle leaves the cluster in which it was originally equilibrated and ends when the residence time of the tagged particle in any of the visited clusters exceeds  $t_{\text{eq}}^*$ . The *net* jump vector is then  $\mathbf{r}_{\text{net}} = \mathbf{R}_{\text{final}}^{\text{cm}} - \mathbf{R}_{\text{initial}}^{\text{cm}}$ , where  $\mathbf{R}_{\text{final}}^{\text{cm}}$  is the CM position of the final cluster site visited during the jump process. This analysis is carried out for all jumping particles in the system and averages are performed over all identified jump events.

The normalized distribution of net jump lengths  $\mathcal{P}_{\text{net}}(r) = \mathcal{P}(|\mathbf{r}_{\text{net}}|)$  is shown in Fig. 4 for the same state point as considered in Fig. 2. The MD results display marked peaks corresponding to integer multiples of the nearest neighbor positions in the fcc lattice, suggesting preferential motion along straight paths. Strikingly, the distribution extends up to and even beyond  $10d_{\text{nn}}$ , where  $d_{\text{nn}}$  is the nearest neighbor distance. That is, particle diffusion in MD simulations proceeds through correlated, long range jumps, whose typical length exceeds  $d_{\text{nn}}$ . The estimated probability of long-range jumps,  $\int_{d_{\text{nn}}}^{\infty} dr \mathcal{P}_{\text{net}}(r)$ , is approximately 50% at the temperature

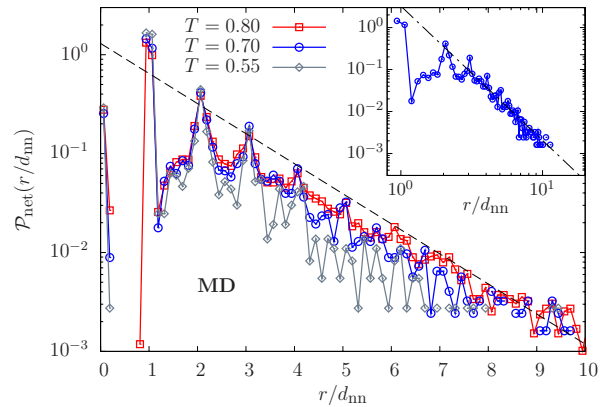


FIG. 5: Main panel: distribution of net jump length  $\mathcal{P}_{\text{net}}$  as a function of  $r/d_{\text{nn}}$  for MD simulations at various temperatures. The dashed line indicates an exponential function  $\sim \exp(-r/\bar{r})$ , with  $\bar{r} \approx 1.43d_{\text{nn}}$ . Inset: log-log plot of  $\mathcal{P}_{\text{net}}(r/d_{\text{nn}})$  for  $T = 0.70$ . The dash-dotted line is a power law decay  $1/r^{1+\alpha}$  with  $\alpha = 2.2 \pm 0.2$ .

considered in Fig. 4, while the estimated probability of jumping to the nearest neighbor site is  $\sim 30\%$ . These values do not depend significantly on temperature (see below). Hence, correlated long-range jumps provide the leading mechanism for mass transport during MD simulations. The shape of the distribution of net jump lengths changes considerably when the MC dynamics is considered. In this case,  $\mathcal{P}_{\text{net}}(r)$  decays rapidly beyond  $r \sim d_{\text{nn}}$ . This can be understood in terms of the stochastic nature of the MC dynamics and suggests that long range jumps in MD simulations are guided by correlations in the momentum direction along the jump path. We will discuss this point in more detail below.

For both types of microscopic dynamics, the net jump length distribution  $\mathcal{P}_{\text{net}}(r)$  displays a mild dependence on temperature. In Fig. 5 we show  $\mathcal{P}_{\text{net}}(r)$  for MD simulations at temperatures  $T = 0.80, 0.70$ , and  $0.55$  for MD simulations. This temperature range corresponds to a variation of diffusivity of approximately three decades (see Fig. 9, further discussed below). In general,  $\mathcal{P}_{\text{net}}(r)$  decays a bit more rapidly as  $T$  decreases. However, the probability of long range jumps in MD simulations remains substantial even at the lowest investigated temperature ( $T = 0.55$ ). Hence, the qualitative differences between MD and MC simulations discussed above with reference to Fig. 4 are relevant for the whole investigated  $T$  range. At large distances ( $r > 2d_{\text{nn}}$ ) the envelope of the maxima of  $\mathcal{P}_{\text{net}}(r)$  obtained from MD simulations can be described reasonably well by an exponential function,  $a \exp(-r/\bar{r})$ , over approximately two decades in  $\mathcal{P}_{\text{net}}(r)$ .  $\bar{r}$  is a characteristic jump length, which depends very weakly on  $T$  and whose value is  $\approx 1.43d_{\text{nn}}$ .

As it can be seen from the inset of Fig. 5, at even larger distances the shape of  $\mathcal{P}_{\text{net}}(r)$  seems to crossover to a power law decay,  $1/r^{1+\alpha}$ , a behavior reminiscent of Levy flights [23, 24]. The estimated power law exponent

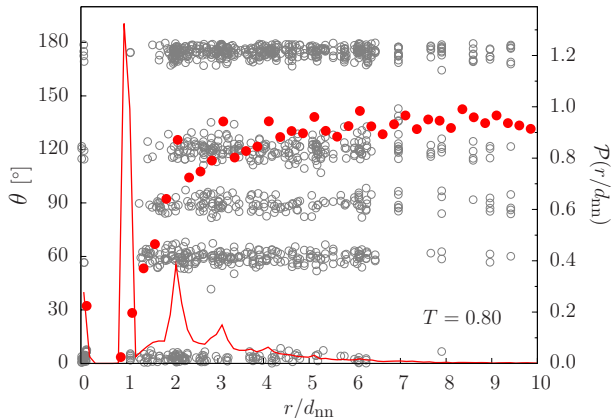


FIG. 6: Correlation between angles  $\theta$  and net jump lengths  $r$  along jump paths at  $T = 0.80$  from MD simulations. Empty circles: angles  $\theta$  between successive jumps versus net jump length  $r$ . Filled circles: correlation between average values of angles at fixed jump length and the jump lengths. The solid line indicates the corresponding distribution of net jump lengths  $\mathcal{P}_{\text{net}}(r/d_{\text{nn}})$  (cf. Fig. 5).

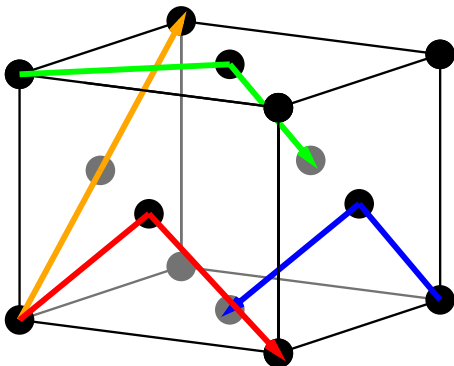


FIG. 7: Possible consecutive jumps to nearest neighbors in the fcc unit cell. The full black and grey circles indicate fcc lattice sites. Blue arrow:  $60^\circ$ ,  $r = d_{\text{nn}}$ . Red arrow:  $90^\circ$ ,  $r = \sqrt{2}d_{\text{nn}}$ . Green arrow:  $120^\circ$ ,  $r = \sqrt{3}d_{\text{nn}}$ . Orange arrow:  $180^\circ$ ,  $r = 2d_{\text{nn}}$ .

$(1 + \alpha \approx 3.2)$  is slightly higher than the upper bound required for standard Levy flights [23, 24]. Furthermore, inspection of the mean square displacement (see Fig. 2) does *not* show clear signatures of anomalous diffusion—a feature commonly associated with Levy flights [23]—on any time scale accessible by our MD simulations. On the basis of the current data, it remains unclear whether a Levy flights picture would be appropriate for the description of diffusion in cluster crystals of ultrasoft particles. More extensive investigations are required to completely settle this issue.

To better characterize the nature of the long range jumps occurring in MD simulations, we now study the relationship between the net jump length  $r$  and the angles  $\theta$  enclosed by successive steps between cluster sites

along the jump path. In Fig. 6 we display the measured angles  $\theta$  versus the corresponding *net* travelled distance  $r$  for a representative state point ( $T = 0.80$ ). For each jump of length  $r$  we stored  $n - 1$  angles, where  $n$  was the number of steps along the path. The horizontal bands at  $60^\circ$ ,  $90^\circ$ ,  $120^\circ$ , and  $180^\circ$  reflect the possible angles between consecutive steps of length  $d_{\text{nn}}$  in the fcc lattice (see Fig. 7). Angles  $\theta \approx 0$  occur for consecutive back and forth steps, while the data at  $r \approx 0$  are associated to jumps, possibly comprising several intermediate steps, whose initial and final clusters coincide.

Fig. 6 shows that the data tend to accumulate at large angles,  $\theta = 180^\circ$  and  $120^\circ$ , corresponding to jumps to second nearest neighbors of the fcc lattice along straight, or slightly deflected, directions. The filled circles in Fig. 6 indicate the average angles at a fixed average net jump length. On average, large angles correspond to large jump lengths, revealing that particles tend to proceed along approximately straight paths, possibly keeping a significant correlation in the direction of their momentum along the jump path. To illustrate the peculiar nature of the hopping processes observed in MD simulations, we show in Fig. 8 the trajectories of selected particles at  $T = 0.80$ . They display correlated jumps over different lengths, ranging from a few nearest neighbor distances (Fig. 8-a) to over  $\sim 10$  nearest neighbor distances (Fig. 8-c). This latter event clearly shows a strong directional correlation of the movement, persisting over several intermediate steps along the jump path.

## B. Diffusion, heterogeneity, and relaxation

Naturally, the question arises: how much are transport properties affected by the difference in the microscopic dynamics? To discuss this point, we compare in Fig. 9 the  $T$ -dependence of the diffusion coefficient  $D$  obtained from MD and MC simulations using the standard Einstein relation, i.e.,  $\langle \delta r^2(t) \rangle = 6Dt$ . As it is customary for systems displaying slow dynamics, the Arrhenius representation is adopted. In the main panel of Fig. 9 the diffusion coefficient for MD,  $D_{\text{MD}}$ , is multiplied by 0.03 for better comparison with the MC data. The fact that it is not possible to present both sets of data on a single curve using a simple rescaling of the time units, demonstrated in the figure by the different slopes of the two data sets, is consistent with the systematic  $T$ -dependence of the ratio of scaling times  $t_{\text{MC}}^*/t_{\text{MD}}^*$  (cf. Fig. 3). This finding is particularly relevant in view of previous numerical investigations on liquids in equilibrium [13, 14] or in the supercooled regime [15–17]. In the latter three studies, MD and Brownian dynamics [16] or MD and MC dynamics [15, 17] were used. It was shown that the long time relaxation of glass-forming liquids is *independent* of the microscopic dynamics. This means that relaxation times, transport coefficients or dynamic correlation functions obtained via the different simulation methods can be superposed after a  $T$ -independent rescaling of the

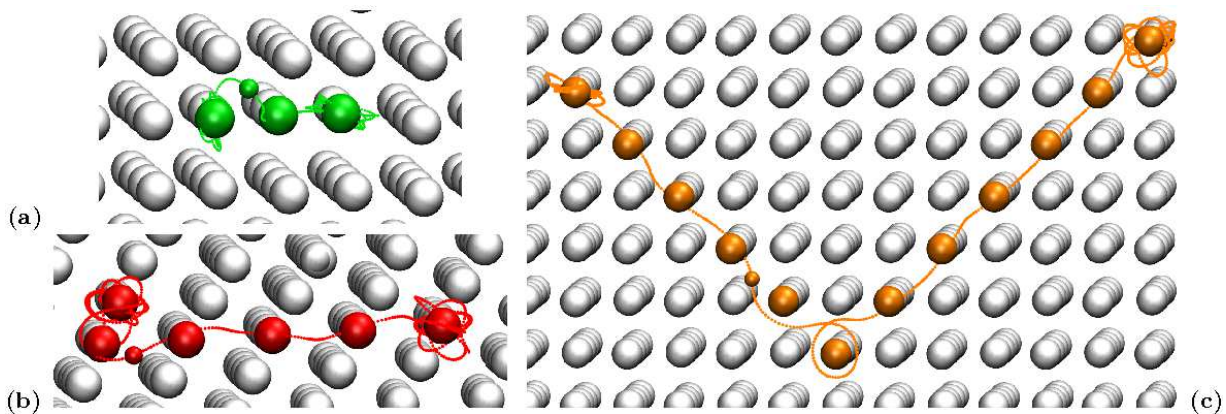


FIG. 8: Representative jump events of tagged particles (indicated by the colored small interstitial sphere) during MD simulations at  $T = 0.80$ . Large particles indicate the centers of mass of the visited cluster sites. The cluster sites visited during the jump path are highlighted with large colored spheres. The positions of the tagged particle along the trajectory are marked at equidistant steps.

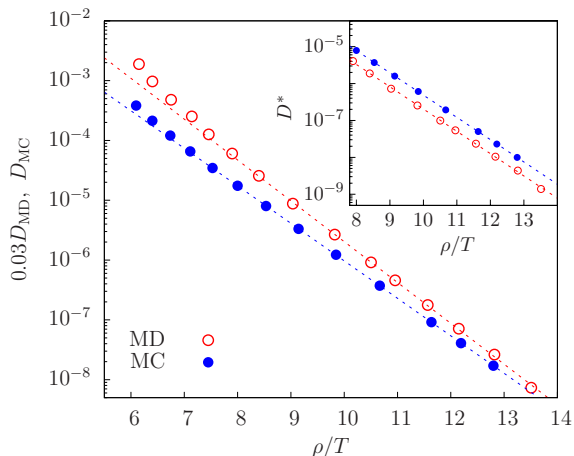


FIG. 9: Main panel: Arrhenius plot of the diffusion coefficient  $D_{MD}$  from MD (empty symbols) and  $D_{MC}$  from MC (filled symbols) simulations. Inset: scaled diffusion coefficients  $D^*$  obtained from MD and MC simulations (see text for definition). In both panels, dotted lines represent fits to the Arrhenius law  $D_0 \exp(-E/T)$ , where  $E$  is an effective activation energy. The activation energy  $E$  equals  $1.57\rho$  and  $1.44\rho$  for fits to  $D_{MD}(T)$  and  $D_{MC}(T)$ , respectively, and  $1.39\rho$  for fits to  $D^*(T)$ , independent of the microscopic dynamics.

time units. For the slow dynamics of ultrasoft particles in cluster crystals, however, such a rescaling approach is hindered due to the prominent role of momentum correlations. Hence, our results indicate that independence of long time relaxation from the microscopic dynamics solely holds for systems where the relevant dynamical correlations are *configurational* in nature.

MD simulations of a GEM-8 cluster crystal [9] have shown that the  $T$ -dependence of  $D$  closely follows the Arrhenius law,  $D = D_0 \exp(-E/T)$ , where  $E = E(\rho)$  is an effective activation energy that scales proportionally

to  $\rho$  [9, 22]. This observation, combined with our analysis of the jump length distributions (Figs. 4 and 5), suggests a way to rationalize the discrepancy between MC and MD results for  $D$ . This can be achieved by invoking a thermally activated diffusion process governed by a unique activation energy, i.e., independent of the microscopic dynamics, but based on different distributions of elementary jump lengths. Towards this aim, let us write down the Arrhenius law for activated diffusion assuming a distribution  $\mathcal{P}_{net}(r)$  of jump lengths

$$D = \frac{\int_0^\infty r^2 \mathcal{P}_{net}(r) dr}{\langle \tau_w \rangle} \exp(-E/T), \quad (2)$$

where  $\langle \tau_w \rangle$  is an average waiting time, which ultimately sets the natural time scale for the process. As long as the  $T$ -dependence of  $\langle \tau_w \rangle$  is approximately similar for the different dynamics, it should be possible to rectify the Arrhenius plots of Fig. 9 by considering the rescaled diffusion coefficient  $D^* = D / \int_0^\infty r^2 \mathcal{P}_{net}(r) dr$ . The inset of Fig. 9 shows that this is indeed the case. Fits to an Arrhenius law for  $D^*(T)$  provide a unique effective activation energy  $E \approx 1.39\rho$ , independent of microscopic dynamics. We found that the fitted value of  $E$  is close to the barrier height  $E_b$  separating neighboring clusters, estimated [22] from single particle potential energies ( $E_b \approx 0.94E$ ). This clearly points to a non-cooperative nature of activated dynamics in the system under consideration.

The microscopic dynamics exerts even a stronger influence on other typical time-dependent correlation functions of the liquid state, such as density-density time correlators. In Fig. 10 we show the self part of the van Hove correlation function  $G_s(r, t)$  at  $T = 0.80$  and compare MD and MC datasets for  $t = t^*$ , where again the scaling time  $t^*$  is chosen such that  $\langle \delta r^2(t^*) \rangle = 25$ . The MC dataset can be simply described by a Gaussian function with variance  $2Dt$  (as expected for standard random walks) modulated by peaks centered at the nearest neigh-

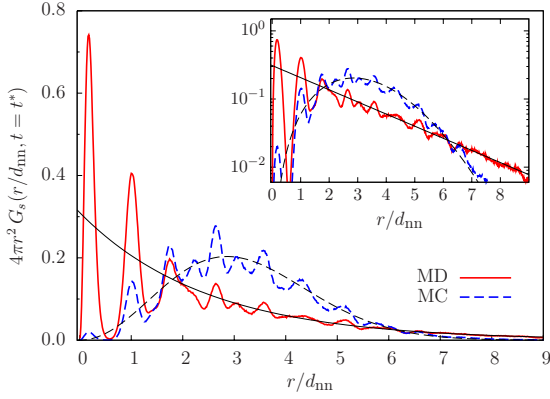


FIG. 10: Main panel: Self part of the van Hove correlation function  $G_s(r, t = t^*)$  as a function of  $r/d_{nn}$  at  $T = 0.80$  for MD (thick solid line) and MC (thick dashed line) simulations. The time  $t^*$  is chosen such that  $\langle \delta r^2(t^*) \rangle = 25$ . The thin dashed line indicates the expected functional form for standard random walk,  $4\pi r^2 \exp[-r^2/(4Dt)]/(4\pi Dt)^{3/2}$ . The thin solid line indicates an exponential function  $\sim \exp(-r/\bar{r})$ , with  $\bar{r} \approx 2.44d_{nn}$ . Inset: same as main plot but on a semi-logarithmic scale.

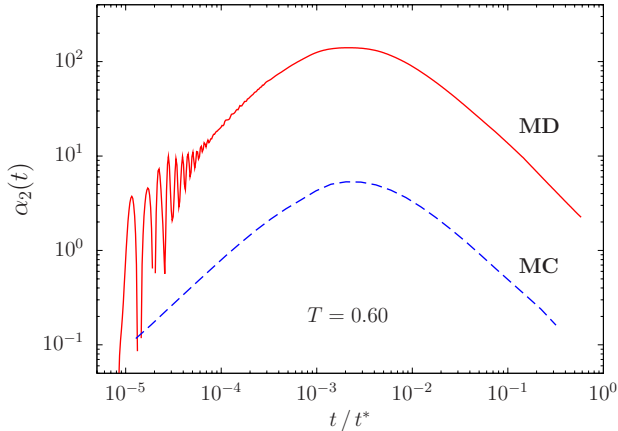


FIG. 11: Non-Gaussian parameter  $\alpha_2$  as defined in Eq. (3) as a function of the rescaled time  $t/t^*$  at  $T = 0.60$  from MD (solid line) and MC (dashed line) simulations with  $t^*$  as defined in the text.

bor distances of the fcc crystal. The MD dataset, on the other hand, is much more stretched and displays an approximately exponential envelope. This behavior is a direct consequence of the broad distribution of elementary jump lengths (cf. Fig. 4 and 5).

The stretched shape of the van Hove correlation function obtained from MD simulations motivates a closer inspection of the non-Gaussian parameter

$$\alpha_2(t) = \frac{3\langle \delta r^4(t) \rangle}{5\langle \delta r^2(t) \rangle^2} - 1, \quad (3)$$

which quantifies the deviation from Gaussianity of the distribution of particle displacements at time  $t$ . In the

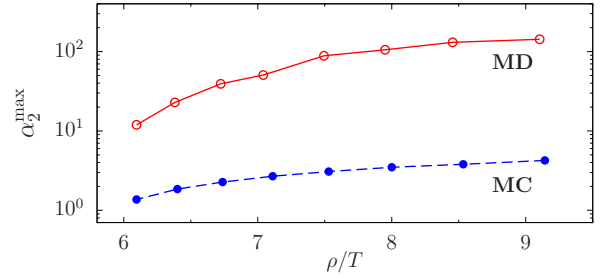


FIG. 12: Maximum value of the non-Gaussian parameter  $\alpha_2^{\max}$  as a function of  $\rho/T$  for MD (empty circles) and MC (filled circles) simulations.

context of glass-forming liquids,  $\alpha_2(t)$  has also been used [25, 26] as a simple measure of “dynamic heterogeneity” [27–29]. In Fig. 11 we show  $\alpha_2(t/t^*)$  at  $T = 0.60$ . At short times qualitative discrepancies appear between MD and MC data, as expected: marked oscillations in  $\alpha_2(t/t^*)$ , due to single-particle vibrations, are observed in fact only for MD simulations. At longer times, on the other hand, the overall shape of  $\alpha_2(t/t^*)$  is very similar to the one found in normal and supercooled liquids [26]: for both types of simulations,  $\alpha_2$  displays a peak at intermediate times corresponding to a maximum value  $\alpha_2^{\max}$ . As in standard glass-formers,  $\alpha_2^{\max}$  grows by decreasing  $T$ , albeit in a moderate fashion (see Fig. 12). However, the values of  $\alpha_2^{\max}$  obtained in MD simulations are significantly larger (up to a factor 40) than in the MC simulations of our system or than the typical values observed in MD simulations of model glass-forming liquids [26]. This is a consequence of the broad distribution of elementary jump lengths found in MD simulations for the system under consideration. Such a dynamic heterogeneity is essentially non-cooperative in origin and therefore different from the one normally observed in glass-forming liquids [27–29]. By visual inspection of animated trajectories, we have checked that jump events are not associated to correlated motions of several particles (as observed, for instance, in [27]), but rather reflect the migration of individual particles over the sample.

Finally, we study the dependence of the self intermediate scattering function

$$F_s(\mathbf{k}, t) = \frac{1}{N} \sum_{j=1}^N \langle \exp\{i\mathbf{k} \cdot [\mathbf{r}_j(t) - \mathbf{r}_j(0)]\} \rangle$$

on the microscopic dynamics. Due to the underlying crystal structure, the relaxation of  $F_s(\mathbf{k}, t)$  is strongly anisotropic, i.e., it depends explicitly on the direction of  $\mathbf{k}$ . While this effect of anisotropy is expected to be most pronounced at reciprocal lattice wave-vectors, we found in addition that  $F_s(\mathbf{k}, t)$  possesses a non-trivial angular dependence at *any* fixed norm (not shown here). To simplify the discussion, in the following we focus only on directions in reciprocal space corresponding to the first and second reciprocal lattice wave-vectors of the fcc lat-

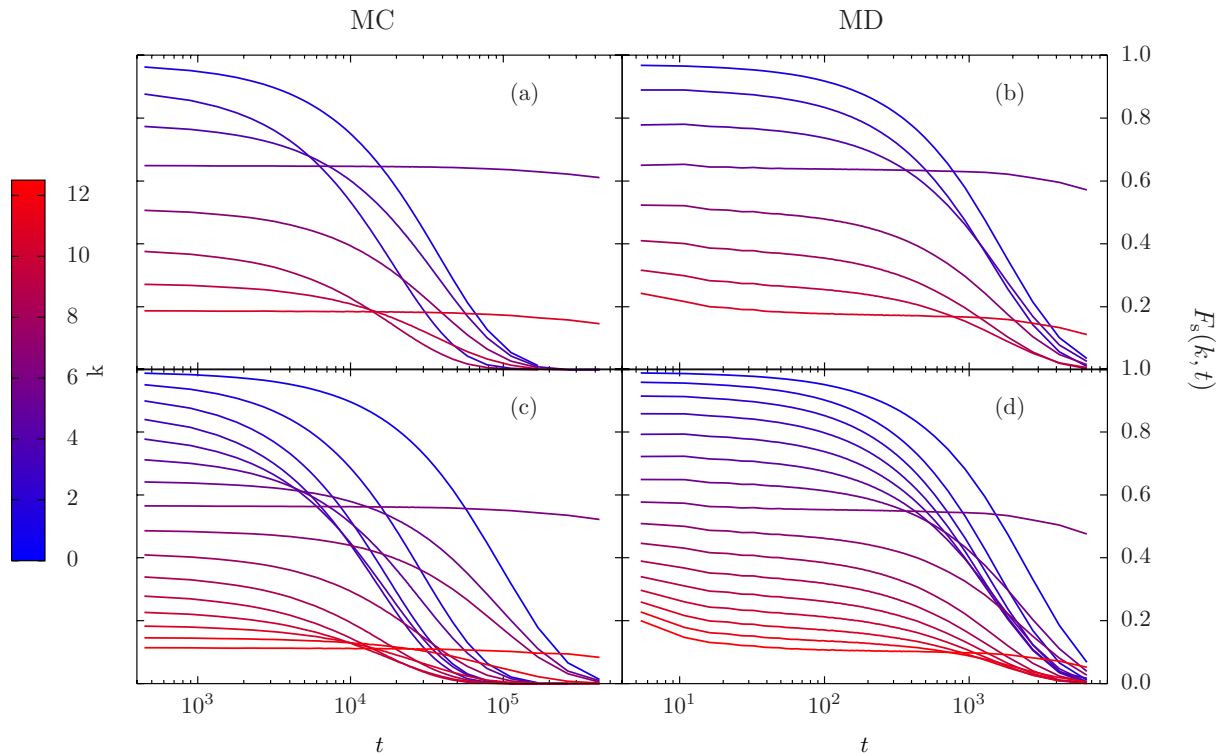


FIG. 13: Self intermediate scattering function  $F_s(\mathbf{k}, t)$  as a function of  $t$  at  $T = 0.80$ . The wave-vectors considered are chosen along the directions  $\mathbf{k}_1$  (panels (a) and (b)) and  $\mathbf{k}_2$  (panels (c) and (d)) corresponding to the first and second reciprocal lattice wave-vectors of the fcc lattice, respectively. The norm of  $\mathbf{k}$  is varied from 0 to  $2k_i$ , with  $i = 1, 2$  (curves from bottom to top); the curves are colored according to the colorscale shown on the left side of the figure. Left and right panels are results from MC and MD simulations, respectively.

tice,  $\mathbf{k}_1/k_1$  and  $\mathbf{k}_2/k_2$ . Along each of these directions, we vary the norm of  $\mathbf{k}$  within the range  $0 < k \leq 2k_i$ , where  $k_i$  is the norm of the selected reciprocal lattice vector ( $k_1 = 5.39$ ,  $k_2 = 6.23$ ). Results obtained at  $T = 0.80$  are collected in Fig. 13. Clearly, the relaxation of  $F_s(\mathbf{k}, t)$  becomes extremely slow at reciprocal lattice vectors. However, the relaxation patterns for off-lattice wave-vectors are rather complex in the two dynamics: as the norm of  $\mathbf{k}$  approaches that of a reciprocal wave-vector the relaxation slows down, but the difference in relaxation times between “fast” and “slow” wave-vectors depends markedly on the microscopic dynamics. Our results indicate a larger heterogeneity of relaxation times for MC dynamics, a fact which contrasts our previous analysis of the non-Gaussian parameter. A similar conclusion is drawn from the analysis of the angular dependence of  $F_s(\mathbf{k}, t)$  at fixed norm of  $\mathbf{k}$  (not shown here). Further investigations are thus required to clarify this behavior and its possible connection to the decoupling between self and collective relaxation discussed in Ref. [9].

### C. Comparison with Brownian dynamics

Our analysis has focused so far on the comparison of dynamical properties obtained through MD and MC simulations. MC simulations are expected to mimic in some sense the Brownian motion of colloidal particles due to collisions with solvent particles. Simulation data [18] and approximate analytical models [20] provide support for this view, at least for small MC displacements. In this subsection we explicitly compare BD and MC simulations for the GEM-4 model, and show that the two methods lead indeed to very similar macroscopic dynamics.

We start with a direct assessment of the net jump length distribution  $\mathcal{P}_{\text{net}}(r/d_{\text{nn}})$  obtained from BD simulations at  $T = 0.60$ . The results are displayed in the main panel of Fig. 14, and compared with the corresponding dataset from MC simulations already presented in Fig. 4. The net jump length distribution from BD simulations is short-ranged and remarkably similar to that obtained using MC simulations. A small peak at  $r \approx 2d_{\text{nn}}$  indicates rare jumps over two nearest neighbor distances, a feature absent in the MC dataset. In the inset of Fig. 14 we show the van Hove correlation function  $G_s(r, t^*)$  calculated at a time  $t^*$  at which the MSD equals 9. We observe a striking correspondence between BD and MC datasets,



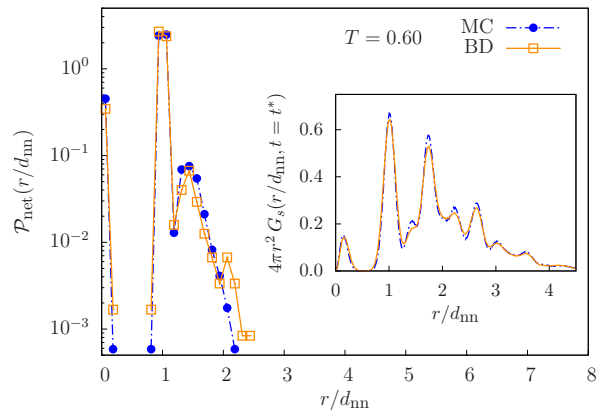


FIG. 14: Main panel: Distribution of net jump length  $\mathcal{P}_{\text{net}}$  as a function of  $r/d_{\text{nn}}$  at  $\rho = 6.4$  and  $T = 0.60$  for BD (empty squares) and MC (filled circles) simulations. Inset: Self part of the van Hove correlation function  $G_s(r, t = t^*)$  as a function of  $r/d_{\text{nn}}$  at  $T = 0.60$  for BD (solid line) and MC (dash-dotted line) simulations. The time  $t^*$  is chosen such that  $\langle \delta r^2(t^*) \rangle = 9$ .

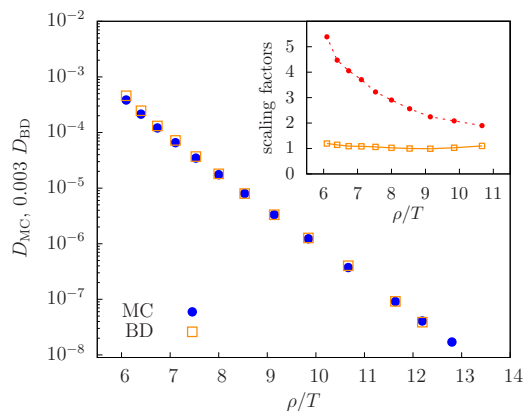


FIG. 15: Main panel: Arrhenius plot of the diffusion coefficient  $0.003 \cdot D_{\text{BD}}$  from BD (empty squares) and  $D_{\text{MC}}$  from MC (filled circles) simulations. The scaling factor for  $D_{\text{BD}}$  has been chosen so as to maximize the overlap of the two data sets. Inset: time scaling factors  $t_{\text{MC}}^*/(t_{\text{MD}}^*/0.003)$  (open squares) and  $t_{\text{MC}}^*/(t_{\text{MD}}^*/\delta t_{\text{MD}})$  (filled circles) as a function of  $\rho/T$ .  $t_{\text{MC}}^*$ ,  $t_{\text{MD}}^*$ , and  $t_{\text{BD}}^*$  are defined as the times at which the mean square displacement equals 4 in MC, MD, and BD simulations, respectively.

demonstrating a close similarity between the dynamics emerging from the two simulation methods.

The temperature dependence of the diffusion coefficient  $D(T)$  is analyzed in Fig. 15 employing the Arrhenius representation. Within the temperature regime explored by BD simulations, the  $T$ -dependences of the diffusion coefficients obtained from BD and MC simulations closely follow one another, up to a trivial, state-independent rescaling of the time unit. Thus, not only the qualitative aspects of transport mechanisms, but also

the  $T$ -dependences of transport coefficients generated by BD and MC are very similar. To contrast the results obtained through these stochastic methods to those of Newtonian dynamics, we report in the inset of Fig. 15 the ratio of the scaling times  $t_{\text{MC}}^*/t_{\text{BD}}^*$  and  $t_{\text{MC}}^*/t_{\text{MD}}^*$ , as defined in Sec. III A. As expected,  $t_{\text{MC}}^*/t_{\text{BD}}^*$  remains fairly constant throughout the available temperature regime. Within the same  $T$ -range,  $t_{\text{MC}}^*/t_{\text{MD}}^*$  displays a systematic variation, as already evidenced in the main panel of Fig. 15.

Overall, the results shown above indicate a strong similarity between the transport mechanisms at play in BD and MC simulations and corroborate the analysis outlined in the previous subsections. In this respect, the results shown in Fig. 14 and 15 support the use of MC simulations as an effective way to incorporate solvent effects in a computer simulation of model colloids [19, 20]. We remark that an attempt to rescale the time unit in our MC simulations by the acceptance ratio, as suggested in [20], resulted in slightly poorer agreement between the two datasets of  $D(T)$ . Thus, more extensive investigations on the connection between dynamical properties generated by MC and BD simulations and possible system-specific aspects are required.

#### IV. CONCLUSIONS AND OUTLOOK

We have performed detailed MD, MC, and BD simulations for ultrasoft particles that form stable clusters of overlapping particles, which, in turn, populate the lattice sites of a regular fcc lattice. Our investigations on the dynamical properties of the system (in terms of particle moves, diffusion and dynamic correlation functions) revealed striking differences between Newtonian and stochastic simulation methods.

(i) In MD simulations, particle diffusion is realized as long-ranged sequences of jumps from one cluster to a neighboring one, assisted by strong correlations in momentum directions. The envelope of the jump length distribution is within a good approximation an exponentially decaying function of the distance and extends up to and beyond ten nearest neighbor distances. At large distances, the jump length distribution is described rather well by a power law,  $1/r^{1+\alpha}$ , with  $\alpha \approx 2.2$ . In MC simulations, by contrast, hopping events are limited to the nearest clusters, as a result of the purely configurational nature of the dynamics. (ii) The diffusion constant,  $D$ , evaluated in MD and MC simulations cannot be matched on a single master curve by a simple rescaling of the respective time units. This finding is in striking contrast to related results obtained in investigations on equilibrated [13, 14] and supercooled [15–17] liquids. However, by normalizing  $D$  with respect to the underlying jump length distribution, an activation energy can be filtered out that is common to both types of dynamics. (iii) Also for the dynamic correlation functions we find distinct differences, which become apparent in the

overall shape of the self part of the van Hove correlation function, in the non-Gaussian parameter, and in the long time decay of the self intermediate scattering function for off-lattice wave vectors. (iv) BD simulations give rise to dynamical properties very similar to those observed during MC simulations, supporting the view that solvent effects are implicitly and effectively included in MC simulations through the stochastic nature of the algorithm.

The present contribution—along with Refs. [9, 10]—can only be considered as a first step towards a deeper understanding of the evidently complex dynamics of cluster forming, ultrasoft systems. Quite a few issues remain unaddressed, which will be dealt with in future contributions. First, a more systematic study of the influence of the solvent, using full Langevin dynamics and possibly including hydrodynamic interactions, is required and will be performed in future work. Other simulation methods, such as dissipative particle dynamics [30, 31], might provide a different, complementary view on our data. Another aspect is related to the underlying model: our inter-particle potential represents an effective interaction between two mesoscopic (colloidal) particles, where the degrees of freedom of the microscopic constituents of the colloids have been traced out [32]. An important issue is thus related to the *level* of coarse-graining, ranging from the present picture of an “effective” particle [12, 32], over partially averaging over sub-entities, such as in multi-blob representations [33], or force-matching schemes [34, 35], to the fully atomistic level where all the constituent entities of the colloidal particles and the particles of the solvent are considered explicitly. Another fundamental question addressing the interpretation of the dynamic correlation functions is how the dynamics of a system of “effective” particles is related to that of a system of atomistically resolved particles.

In conclusion, our work has revealed qualitative differences in the dynamics of ultrasoft, cluster-forming particles obtained using Newtonian and two stochastic (i.e., Brownian dynamics and Monte Carlo) simulation methods. This effect has been attributed to the competition between activated processes and solvent effects, which controls the distribution of jump lengths and ultimately the dynamic correlation functions. We speculate that the interplay between activated slow dynamics and solvent effects could generate complex dynamical scenarios in ultrasoft colloids, such as dendrimers and microgels, and even a broader class of cluster-forming colloids, including systems with competing interactions. With this contribution we hope to motivate further numerical and experimental studies on the dynamics of such colloidal systems to test this hypothesis.

### Acknowledgments

We thank B. M. Mladek, D. Frenkel, C. N. Likos, W. Kob, F. Colonna for useful comments and discussions. We also thank C. N. Likos for a critical reading of the

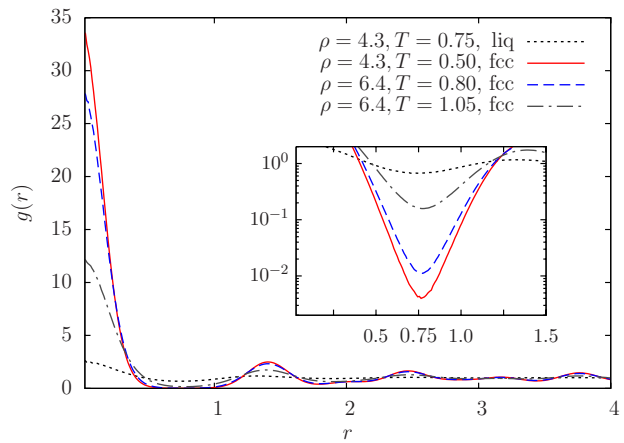


FIG. 16: Radial distribution function,  $g(r)$ , of a GEM-4 system as a function of  $r$  for different densities  $\rho$  and temperatures  $T$ , both in the liquid and fcc cluster crystal phase. From the inset we see that  $g(r)$  does not vanish completely at its first minimum,  $r_{\min} \approx 0.75$ .

manuscript. Financial support by the Austrian Science Fund (FWF) under project P19890-N16 and the Center for Computational Materials Science (CMS) is acknowledged.

### Appendix A: Cluster identification algorithm

In an effort to trace the migration of the particles through the cluster crystal we developed an algorithm to distinguish between different clusters and to identify the affiliation of a particular particle to a cluster in an unambiguous way at every step of the simulation. In previous investigations on clustering systems [7], the position of the first minimum in the pair distribution function  $g(r)$ ,  $r_{\min}$ , was used to provide information whether two particles, separated by a distance  $r$ , belong to the same cluster (for  $r \leq r_{\min}$ ) or not (for  $r > r_{\min}$ ). This criterion can undoubtedly be used to obtain a first, rough estimate for identifying those particles that belong to a particular cluster. However, a closer analysis of  $g(r)$  reveals (cf. Fig. 16) that even for relatively low temperatures this function does not vanish completely for  $r \sim r_{\min}$ . Particles migrating between two neighboring cluster sites of the cluster crystals are to be made responsible for this effect.

In the following we present a refined version of the cluster identification algorithm presented in Ref. [7]; it can be subdivided into the following four steps:

1. We start our procedure with the first particle and identify all particles separated by a distance less than a given cut-off radius  $r_c$  as neighboring particles. This procedure is repeated for all remaining particles. As a first guess we choose  $r_c = r_{\min}$ , a value which will be corrected iteratively during this

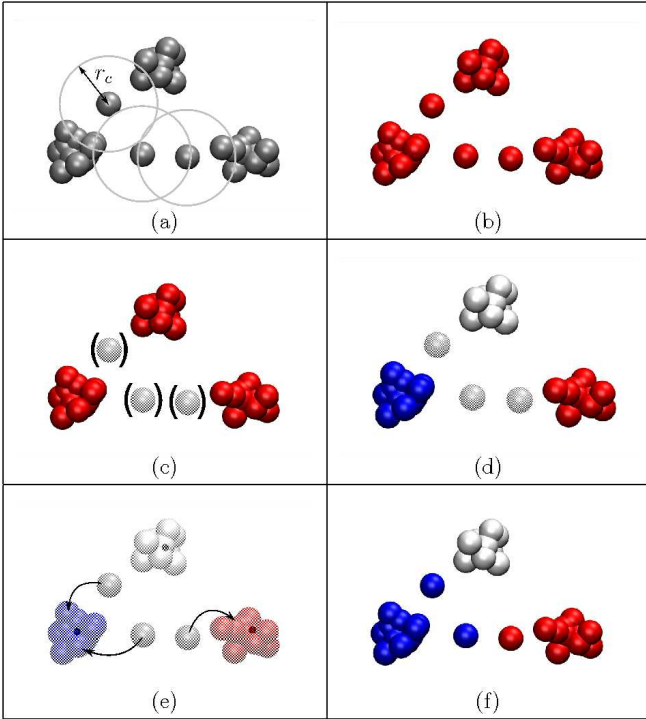


FIG. 17: Procedure to separate merged clusters. (a) Three neighboring clusters are merged by hopping particles. At this step, all particles in red form a single cluster. (b) The search for particle neighbors is repeated for the merged cluster with a reduced cut-off radius  $r_c$ . (c) Particles (light grey spheres) with a small number of neighbors ( $n_c < n_c^{\min}$ ) are excluded. (d) The search for particle neighbors is repeated ignoring the light grey spheres, identifying thereby disjoint clusters. (e) Excluded particles (light grey spheres) are reintroduced and reassigned to the respective nearest clusters. (f) Procedure accomplished, yielding three disjoint clusters.

algorithm.

2. With this information at hand, we start again with the first particle and label all its neighbors, their respective neighbors, etc.; in this way, we are able to identify a first cluster of the system. We then proceed to the next particle that has not been labelled yet, and repeat the operation. Finally, all particles have been assigned to a cluster.
3. At this stage, the algorithm reproduces exactly the results obtained in [7]. It risks, however, to provide misleading data: as particles move from one cluster to another, the particles of these two clusters might now be counted to belong to the set of neighbors of the hopping particle, merging thereby the two clusters (see Fig. 17-a). In our refined algorithm, we modify the first guess of  $r_c$  in an iterative way and eventually all merged clusters and all single-particle clusters are eliminated. To this end, we reduce  $r_c$  and introduce three check parameters:  $n_c^{\min}$  and  $n_c^{\max}$ , the expected minimum and max-

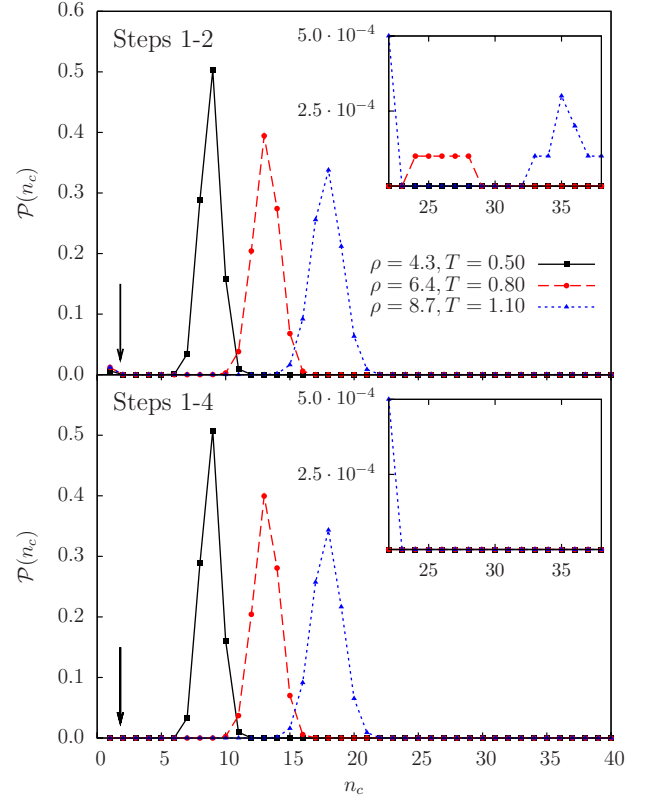


FIG. 18: Distribution of cluster sizes  $n_c$  for various state points. Upper panel: distribution calculated after Step 2 of the cluster analysis algorithm. The inset shows an enlargement of the large- $n_c$  region, revealing the occurrence of merged clusters. The arrow indicates the occurrence of clusters composed by few particles. Lower panel: distribution calculated after Step 4. The inset reveals the absence of merged clusters. The arrow indicates that all clusters of size less than  $n_c^{\min}$  have vanished.

imum cluster size present in our system (roughly estimated from the cluster size distribution calculated after Steps 1 and 2) and  $N_c$ , the number of lattice sites in our system which is, by definition, equal to the amount of clusters in the crystal phase.

We proceed as follows: all clusters that have just been identified are re-considered. If the size of one of them exceeds  $n_c^{\max}$ , the corresponding collection of particles is isolated from the rest of the system (see Fig. 17-a) and the search for neighbors is repeated within the remaining set of particles (Fig. 17-b). In a similar manner, those particles with the lowest number of neighbors are also isolated from the others (Fig. 17-c) since these particles are found to be responsible for merging neighboring clusters. Ignoring the excluded particles for a moment, the neighbors are identified once again

as described above (cf. Step 2), giving disjoint clusters (Fig 17-d). Now the isolated particles are re-integrated into the ensemble and are reassigned to those clusters with the nearest center of mass position (Fig. 17-e and 17-f). Finally, the following checks are made: (i) Does the size of all newly established clusters lie within  $n_c^{\max}$  and  $n_c^{\min}$ ? (ii) Is the number of clusters identified in the system equal to the number of lattice sites,  $N_c$ ? If one of these two conditions is violated, the procedure is iterated reducing the cut-off radius  $r_c$  at each iteration step.

4. In a final check on the size of the clusters, those particles or small collections of particles that possibly have not been assigned to none of the clusters before, are assigned to the cluster with the nearest center of mass. The success of the improved cluster analysis algorithm becomes obvious from the

ensuing cluster population distribution. Peaks due to single particles and merged clusters have vanished (see Fig. 18, right panel), reflecting the correct analysis of the cluster sizes distribution of the system.

Finally, to match the identity of clusters at different times, we exploit the fact that in the *crystal phase* the centers of mass of the clusters are fixed to their respective lattice sites. To be more specific, we found that the root mean square displacement of the centers of mass does not exceed ten percent of the nearest-neighbor distance between clusters,  $d_{nn}$ , at any state point in the fcc region of the phase diagram. We can thus keep track of the identity of any selected cluster by locating the cluster that, at the next time step, has the closest center of mass and by repeating this operation for all time steps.

- 
- [1] W. Klein, H. Gould, R. A. Ramos, I. Clejan and A. I. Mel'cuk, *Physica A*, 1994, **205**, 738.
  - [2] W. Klein, H. Gould, R. A. Ramos, I. Clejan and A. I. Mel'cuk, *Phys. Rev. E*, 2000, **63**, 031206.
  - [3] B. M. Mladek, D. Gottwald, G. Kahl, M. Neumann and C. N. Likos, *Phys. Rev. Lett.*, 2006, **96**, 045701.
  - [4] B. M. Mladek, D. Gottwald, G. Kahl, M. Neumann and C. N. Likos, *Phys. Rev. Lett.*, 2006, **97**, 019901.
  - [5] C. N. Likos, B. M. Mladek, D. Gottwald and G. Kahl, *J. Chem. Phys.*, 2007, **126**, 224502.
  - [6] B. M. Mladek, P. Charbonneau, C. N. Likos, D. Frenkel and G. Kahl, *J. Phys.: Condens. Matter*, 2008, **20**, 494245.
  - [7] B. M. Mladek, D. Gottwald, G. Kahl, M. Neumann and C. N. Likos, *J. Phys. Chem. B*, 2007, **111**, 12799.
  - [8] B. M. Mladek, P. Charbonneau and D. Frenkel, *Phys. Rev. Lett.*, 2007, **99**, 235702.
  - [9] A. J. Moreno and C. N. Likos, *Phys. Rev. Lett.*, 2007, **99**, 107801.
  - [10] C. N. Likos, B. M. Mladek, A. J. Moreno, D. Gottwald and G. Kahl, *Comp. Phys. Comm.*, 2008, **179**, 71.
  - [11] A. A. Louis, P. G. Bolhuis, J. P. Hansen and E. J. Meijer, *Phys. Rev. Lett.*, 2000, **85**, 2522.
  - [12] B. M. Mladek, G. Kahl and C. N. Likos, *Phys. Rev. Lett.*, 2008, **100**, 028301.
  - [13] H. E. A. Huitema and J. P. van der Eerden, *J. Chem. Phys.*, 1999, **110**, 3267.
  - [14] G. Rutkai and T. Kristof, *J. Chem. Phys.*, 2010, **132**, 104107.
  - [15] L. Berthier and W. Kob, *J. Phys.: Condens. Matter*, 2007, **19**, 205130.
  - [16] T. Gleim, W. Kob and K. Binder, *Phys. Rev. Lett.*, 1998, **81**, 4404.
  - [17] L. Berthier, *Phys. Rev. E*, 2007, **76**, 011507.
  - [18] K. Kikuchi, M. Yoshida, T. Maekawa and H. Watanabe, *Chem. Phys. Lett.*, 1991, **185**, 335.
  - [19] G. Brambilla, D. E. Masri, M. Pierno, L. Berthier, L. Cipelletti, G. Petekidis and A. B. Schofield, *Phys. Rev. Lett.*, 2009, **102**, 085703.
  - [20] E. Sanz and D. Marenduzzo, *J. Chem. Phys.*, 2010, **132**, 194102.
  - [21] M. P. Allen and D. J. Tildesley, *Computer Simulation of Liquids*, Clarendon Press, Oxford, 1987.
  - [22] L. Strauss, *M.Sc. thesis*, Technische Universität Wien, 2009.
  - [23] M. F. Shlesinger, G. M. Zaslavsky and J. Klafter, *Nature*, 1993, **363**, 31.
  - [24] G. M. Zaslavsky, *Phys. Rep.*, 2002, **371**, 461.
  - [25] M. Vogel and S. C. Glotzer, *Phys. Rev. E*, 2004, **70**, 061504.
  - [26] D. Coslovich and G. Pastore, *J. Phys.: Condens. Matter*, 2009, **21**, 285107.
  - [27] C. Donati, J. F. Douglas, W. Kob, S. J. Plimpton, P. H. Poole and S. C. Glotzer, *Phys. Rev. Lett.*, 1998, **80**, 2338.
  - [28] A. Widmer-Cooper, P. Harrowell and H. Fynewever, *Phys. Rev. Lett.*, 2004, **93**, 135701.
  - [29] G. A. Appignanesi, J. A. R. Fris, R. A. Montani and W. Kob, *Phys. Rev. Lett.*, 2006, **96**, 057801.
  - [30] P. J. Hoogerbrugge and J. M. V. A. Koelman, *Europhys. Lett.*, 1992, **19**, 155.
  - [31] P. Nikunen, M. Karttunen and I. Vattulainen, *Comp. Phys. Comm.*, 2003, **153**, 407.
  - [32] C. N. Likos, *Phys. Rep.*, 2001, **348**, 267.
  - [33] C. Pierleoni, B. Capone and J.-P. Hansen, *J. Chem. Phys.*, 2007, **127**, 171102.
  - [34] S. Izvekov and G. A. Voth, *J. Chem. Phys.*, 2005, **123**, 134105.
  - [35] W. G. Noid, J. Chu, G. S. Ayton, V. Krishna, S. Izvekov, G. A. Voth, A. Das and H. C. Andersen, *J. Chem. Phys.*, 2008, **128**, 244114.